Detecting Dynamic Causal Inference in Nonlinear Two-Phase Fracture Flow

Boris Faybishenko
Energy Geosciences Division
Earth and Environmental Sciences Area
Lawrence Berkeley National Laboratory
University of California, Berkeley
Berkeley, CA 94720
bafaybishenko@lbl.gov

Abstract

Identifying dynamic causal inference involved in flow and transport processes in complex fractured-porous media is generally a challenging task, because nonlinear and chaotic variables may be positively coupled or correlated for some periods of time, but can then become spontaneously decoupled or non-correlated. In his 2002 paper (Faybishenko, 2002), the author performed a nonlinear dynamical and chaotic analysis of time-series data obtained from the fracture flow experiment conducted by Persoff and Pruess (1995), and, based on the visual examination of time series data, hypothesized that the observed pressure oscillations at both inlet and outlet edges of the fracture result from a superposition of both forward and return waves of pressure propagation through the fracture. In the current paper, the author explores an application of a combination of methods for detecting nonlinear chaotic dynamics behavior along with the multivariate Granger Causality (G-causality) time series test. Based on the G-causality test, the author infers that his hypothesis is correct, and presents a causation loop diagram of the spatial-temporal distribution of gas, liquid, and capillary pressures measured at the inlet and outlet of the fracture. The causal modeling approach can be used for the analysis of other hydrological processes, for example, infiltration and pumping tests in heterogeneous subsurface media, and climatic processes, for example, to find correlations between various meteorological parameters, such as temperature, solar radiation, barometric pressure, etc.

Keywords: Two-phase fracture flow; nonlinear dynamics; time series; capillary pressure; Granger causality; causality loop diagram.

1. Introduction

It is well established that nonlinearity is often a typical feature of many ecological processes (e.g., Casini et al., 2009; Sugihara and May, 1990; Dixon et al., 1999).

Nonlinearity is also known to exist for flow in hydrological systems (Perfect, 1997; Weeks and Sposito, 1998; Pasternack, 1999; Sposito, 1999; Sivakumar, 2000) and fractured-porous media (Faybishenko, 2002; 2003). Since the work of French mathematician Henri Poincaré, it has also been known that nonlinear deterministic systems can behave in an apparently unpredictable, chaotic manner. Chaotic phenomena are widespread in all fields of sciences, including physics (Abarbanel, 1996), chemistry (Winfree, 1984), biology (May, 1974; Skarda & Freeman, 1987), psychology (Guastello et al., 2009), ecology (Nicolis, 1991; Benincà et al., 2008; Cushing et al., 2003), etc. The principal source of difficulties in analyzing hydrological models is the extreme variety, variability, and complexity of processes that affect hydrologic phenomena, which require the knowledge of different temporal and spatial scales of these processes and their interactions, temporal and spatial irregularities and instabilities, requiring the application of empirical and causal models in hydrology (Klemes, 1982; Gilvear et al., 2016). Because of these difficulties, identifying the causality, i.e., the cause-effect of multiple variables, in complex hydrological systems is generally a difficult task, because variables that may be positively coupled or correlated for some periods of time can then become spontaneously decoupled or non-correlated due to chaotic nature of underlying processes. For most flow and transport problems in fractured rock, it is not possible to develop models directly from first principles (Pruess et al., 1999; Faybishenko, 2002), and is not possible to develop mathematical models, using systems of partial differential equations, to be used for predictions (Committee on Major U.S. Oceanographic…, 1999).

Over the last 30-40 years, there has been a great deal of field, laboratory, and modeling research in fractured-rock hydrogeology [e.g., Bear et al., National Research Council, Faybishenko et al. [2000; 2016; Nicholl et al., 1994] concerning the spatial and temporal instabilities of flow in unsaturated media. Despite of many publications, the physics of such flow remains unclear. In his previous publications the author showed that the unsaturated fractured-rock system is chaotic because the flow processes are nonlinear, sensitive to initial conditions, and dissipative, and confirmed that the presence of chaotic behavior by calculating diagnostic chaotic parameters for gas, liquid, and capillary pressures, measured during the water–gas injection in fractures, as well as laboratory and field dripping-water experiments. These results revealed the presence of deterministic chaos in the intra-fracture flow processes accompanied by a random component. Deterministic chaos, in conjunction with noise effects, creates a source of irreducible uncertainty for long-term predictions, which implies that the predictability of a chaotic system cannot be improved by making more precise measurements of initial conditions and system parameters. Deterministic chaotic modes can provide meaningful predictions for a limited time duration, after which only stochastic models can be used [Schuster, 1989]. Moreover, for nonlinear dynamical processes, a lack of correlation, which is some time determined using conventional statistical methods, does not imply the lack of causation. Conversely, the presence of correlation does not imply the presence of real physical relationship between the variables. For example, using the results of the fracture flow test (Persoff and Pruess, 1995), the author (Faybishenko, 2002) examined the time series of inlet and outlet gas and liquid pressure oscillations,

and showed that the pressure buildup first begins at the inlet and then propagates to the outlet of the fracture. This pattern means that a pressure-wave propagates forward as the water-air mixture moves from the inlet to the outlet of the fracture. Theoretically, the amplitude of forward and return waves must decay in the direction of flow, implying the dispersion of flow (Rabinovich and Trubetskov, 1994, p. 228). However, the pressure drop first begins at the outlet and then propagates backward to the inlet. The author hypothesized that the observed quasi-periodic pressure oscillations at both inlet and outlet ends of the fracture result from a superposition of both forward and return waves of pressure propagation through the fracture. However, no quantitative evaluation of these phenomena of directional influences in fracture flow has yet been given.

The objective of this paper is to quantitatively characterize the interconnection between the inlet and outlet gas, liquid, and capillary pressure measurements, using a combination of methods of detecting chaotic behavior and the Granger causality (GC) testing of multivariable time series, based on the gas and water measurements in flowing fracture. The structure of the paper is as follows. Section 2 includes a brief description of the Persoff-Pruess experiment and the results of the nonlinear dynamics analysis of time series gas and liquid inlet and outlet pressures and capillary pressures. Section 3 provides a description of the methods used for causality testing in this paper. Section 4 includes a discussion of the results of calculations, including a presentation of the causality loop diagram, and Section 5 presents conclusions and directions of future research.

2. Brief description of the fracture flow experiment and evaluation of diagnostic parameters of nonlinear dynamics

2.1. Persoff and Pruess (1995) Experiment

Persoff and Pruess (1995) conducted a series of two-phase flow experiments by simultaneously injecting water and nitrogen gas (respectfully, wetting and nonwetting phases) into replicas of natural rough-walled rock fractures in granite (from the Stripa mine in Sweden) and tuff (from Dixie Valley, Nevada). The scheme of the experimental design and measurements is shown in Figure 1. Gas was injected at the inlet edge to a plenum that distributed gas to a set of 40 vertical grooves in the porous block. Gas and liquid pressures at the inlet and outlet edges of the fracture were measured for a series of constant flow rates. Capillary pressure was measured using the differential pressure transducers installed at the inlet and outlet edges of the fracture. Assuming fractures as homogeneous porous media, and using averaged pressures, liquid and gas relative permeability functions were calculated based on the theory of Darcy flow. In this paper, we will analyze the results of Experiment C, which was carried out using the Stripa natural rock (fracture hydrodynamic aperture 21.7 μm) with a gas flow rate of 0.52 cm^3/min (measured at standard conditions), and a liquid flow rate of 0.25 cm^3/min (the gas-liquid volumetric flow ratio is approximately 2), and the Reynolds numbers was

much less than 1.

2.2. Time Series of Gas and Liquid Pressures

Figure 2 shows measured gas and liquid pressure time series, which were collected every 0.4 sec. Figure 3 demonstrates differential gas and liquid pressures along the length of the fracture (determined using differential pressure transducers installed between inlet and outlet gas pressures), and reveals that the drop in the liquid pressure corresponds to the spike in the gas pressure. The sharp drops in the gas differential pressure occurred at the time of the increase in the differential liquid pressure. Instabilities in the liquid and air pressures, observed under constant liquid and gas injection rates, were likely resulted from recurring changes in phase occupancy between liquid and gas at a critical pore throat in a fracture, as well as a competition between fluid pressures caused by injection and capillary effects driving the liquid to the critical throat (Persoff and Pruess, 1995).

The time series data were used for a pair-wise comparison of measured gas ($P_{g.in}$) and liquid ($P_{l.in}$) pressures, which is shown in Figure 4 by plotting two-dimensional scatterplots, i.e., phase-space attractors. Figure 4a shows that the inlet gas-liquid pressure ($P_{g.in}$ vs. $P._{l.in}$) attractor (black color) is only slightly skewed from the 1:1 line (thin black line), and is located in the area of greater values of the pressures. The shape of the outlet gas-liquid attractor (green color) is different: it is practically horizontal (extended in the *x* direction along the gas pressure coordinate), and narrower in the *y* direction (i.e., liquid pressure); the outlet attractor is located in the area of lower values of the pressures – the lower pressures at the outlet are expected due to flow from the inlet to the outlet.

Figure 4b shows the scatterplots/attractors of the gas inlet ($P_{g.in}$) – gas outlet ($P_{g.out}$) pressures and liquid inlet ($P_{l.in}$) – liquid outlet ($P_{l.out}$) pressures. One can see a narrower scatterplot, close to a linear relationship, of the inlet-outlet liquid pressure, and a much more scattered plot of the inlet-outlet gas pressures. One can see that both plots are shifted from the 1:1 line, because the inlet pressures exceed the outlet pressures.

Figure 5 illustrates the time variations of the capillary pressures at the inlet and outlet of the fracture, which were measured using differential pressure transducers between the gas and liquid ports. This figure shows that relatively short periods of laminar flow, when the capillary pressure was negative (shown in Figure 5 below the line $P_{cap} = 0$), are interrupted by chaotic surges in the capillary pressure, when the capillary pressure increased to positive values. Persoff and Pruess (1995) suggested that the pressure changes resulted from recurring blockage of critical pore throats and phase changes between water and gas, and the rapid drop in capillary pressure at the end of each chaotic phase is likely caused by liquid breakthrough through a pore throat. Figure 5 also demonstrates a larger magnitude of the outlet capillary pressure fluctuations than that at the inlet, probably caused by a larger positive pressure build-up near the

fracture's outlet. Although the inlet gas and liquid pressure fluctuations exhibit identical quasi-periodic cycling fluctuations, with a small time-delay of the liquid pressure during the period of the pressure increase. (This time delay can also be caused by the time delay in pressure measurements, using a porous cup with lower permeability than the time delay of air-pressure sensors.)

Theoretically, the amplitude of forward and return waves of the pressure must decay in the direction of flow, implying the dispersion of flow (Rabinovich and Trubetskov, 1994, p. 228). However, Figure 6 demonstrates that the pressure build up first begins at the outlet and then propagates backward to the inlet—see the arrows on both upper and lower plots of Figure 6. Following the discussion in Faybishenko (2002), we hypothesize that the observed pressure oscillations at both inlet and outlet of the fracture result from a superposition of both forward and return waves of pressure propagation through the fracture. (Note: a comparison of the capillary pressure measured using pressure transducers and calculated as a difference between the recorded gas and liquid pressures will be given in a separate paper. In this paper, the author analyzed the capillary pressure measured during the experiment.)

2.3. Diagnostic nonlinear dynamics parameters of time series

It is often assumed in hydrological investigations that high frequency oscillations represent a noisy signal produced by improperly tagged data or errors of measurements, but not by physical phenomena. The author previously (Faybishenko (2002) analyzed the inlet and outlet gas, liquid, and capillary pressures and showed the presence of nonlinear deterministic chaotic phenomena after filtering time series by means of a low-pass technique to remove high-frequency oscillations. However, removing high-frequency oscillations may cause spurious cause-effect correlations between the variables. Therefore, in this paper, the author assumed that the analysis of the directly measured data would provide added benefits to achieving the goal of the current paper to assess the interconnection between the variables in the presence of chaotic dynamics. The following diagnostic nonlinear dynamics parameters were calculated based on the time delay of time series (determined using the averaged mutual information—AMI): global (D_{GED}) and local embedding dimensions determined using the False Nearest Neighbor (FNN) method, the correlation dimension (D_{cor}), Lyapunov exponents, and information dimension (D_{inf}). Calculations were conducted with the application of the R code "Fractal." The results of calculations shown in Figures 7 though 9 and Table 1 for the inlet and outlet capillary pressures demonstrate evidence of low dimensional chaotic behavior, with D_{GED} from 4 to 5, D_{cor} from 1.57 to 2.62, positive values of the maximum Lyapunov exponents, and negative sums of the Lyapunov exponents (indicating that the systems embedding attractors are converging), and D_{inf} between 2 and 3. The 3-D pseudo-phase attractors were plotted using the time lags calculated from the AMI analysis. These 3-D attractors represent approximations of higher order (D_{EMD} = 4 and 5) processes.

3. Evaluation of Causality

3.1. Philosophical primer of the principle of causality

Recently, there has been considerable interest in a class of techniques called Granger causality, which can help provide a statistically reliable approach to assess multi-parameter influences in complex systems of different origin (e.g., Granger, 1969; 1980; Dixon et al., 1999; Deyle and Sugihara, 2011; Sugihara et al., 2012). The principle of causality is, generally, a well-known philosophy concept, which is also called a concept of "cause" and "effect" (Bohm, 1957, Spirkin, 1990). This concept can be used for the evaluation of the coupling between simultaneously occurring temporal events, which could be contiguous events or events affected by the same cause. The cause and effect of some system's variables can be distributed over the time, and can be either divided by a time interval or connected through other intermediate system's links or variables. The coupling between the system's cause and effect may be expressed as follows: if A is the cause of B, and B is the cause of C, then A may also be considered as the cause of C. An effect may have several causes—some principal, and some accidental or secondary. If the network of causal links between the systems components is continuous, with no internal interruptions, the law of conservation of matter and motion is valid (i.e., Spirkin, 1990). In this case, the system's internal mechanisms of causality are related to each other, causing the processes of transfer of matter, motion and information, as well as producing both feedback and forward feed in the system. The natural system behavior is induced by the interaction of at least two phenomena or processes, so that the causality process forms the system's structural organization. Practically, we need to identify a finite number of significant primary and secondary interactions to characterize the system's behavior and organization. Often, direct causes could be difficult to distinguish from secondary causes, which, in turn, could be related through a number of intervening (and often not known) processes. It is important that a cause can essentially take effect on the system when specific conditions (thresholds) are met. The problem of the physical nonlinear relationship between cause, condition, and effect can be solved differently, depending on the complexity of the system's relationships, the ability to distinguish a comparative importance and to determine the correlation between multiple factors and processes. Due to the nonlinear relationship between the system variables, the variables may show a spurious relationship and the causally between several variables may be very complex. Apparent relationships among variables can switch spontaneously in nonlinear systems as a result of mirage correlations or a threshold change in regime. The approach to assess the causality between the system's variables is described in Section 3.2.

3.2. Granger causality approach

The Granger causality (GC) test has been recognized as the primary test on the causation problem, since publications by Granger (1969; 1980, 1988), who introduced a definition of the concept of causality that does not rely on the specification of a specific scientific model. This definition is particularly suited for interpretation of empirical cause-effect relationships. The GC approach provides a conceptual framework of using predictability, not a correlation approach, to identify causation between time-series variables. The Granger causality addresses the issue with prediction rather than correlation as the criterion for causation in time series. Variable X is said to "Granger cause" (G-cause) Y, if the predictability of Y declines when X is removed from the universe of all possible causative variables (Granger, 1969). According Granger (1969), the application of this approach may be problematic for deterministic dynamic systems with weak to moderate coupling. For example, in deterministic or stochastic dynamic systems, if X is a cause for Y, information about X will be redundantly present in Y itself and cannot formally be removed (Sugihara et al., 2012). According to the dynamical systems theory, time-series variables are causally linked if they are from the same dynamic system (Dixon et al., 1999; Deyle and Sugihara, 2011). These variables share a common attractor manifold, so that each variable can identify the state of the other (Packard et al., 1980; Sugihara and May, 1990; Abarbanel, 1996). Granger defined the causality relationship based on two principles (Granger, 1980; Eichler, 2012):

- Temporal precedence, when causes precede their effects, and
- Physical influence, if manipulation of the cause changes the effects.

The theoretical basis for the Grarger-causality approach is the cause happens prior to its effect, the cause and its effect are uniquely linked, and the cause contains the information about the future values of its effect. A conceptual idea of the multivariate Granger causality analysis is to perform the fitting of a vector autoregressive model (VAR) to the time series. For instance, for $X(t) \in R^{d\times 1}$ for t = 1, …, T, which is a d-dimensional multivariate time series, the Granger causality is assessed by fitting a VAR model with L time lags as follows (Lütkepohl, 2005)

$$X\ (t) = \sum_{\tau=1}^{L} A_\tau X(t-\tau) + \varepsilon(t)$$

where $\varepsilon(t)$ is a white Gaussian random vector, and a time series X_i is called a Granger cause of another time series X_j, if at least one of the elements $A_\tau(i,j)$ for □ = 1,⋯, L significantly larger (in absolute value) than zero. The F-statistic is applied to assess a rejection of the null hypothesis that there is Granger causality. The null hypothesis that X_i does not Granger-cause X_j is not rejected if and only if no lagged values of X_i are retained in the regression. In this paper, the multivariate Granger causality analysis was performed using the time lags determined the AMI analysis given in Section 2.2.

One of the conditions to apply the Granger-causality test is the statistical stationarity of the time series variable. To assess the stationary the Kwiatkowski–Phillips–Schmidt–Shin (KPSS) test was first applied (using the R library "urca") for a null hypothesis that an observable time series is stationary around a deterministic trend, i.e. trend-stationary, against the alternative of a unit root (Pfaff et al., 2016). The null hypothesis of the stationarity around a constant mean was tested against the alternative that the series is not stationary (i.e., of integration order I(1)). The results are summarized in Table 2, indicating the stationarity of the time series. (The Augmented Dickey–Fuller (ADF) statistics test was also applied, using the R library "tseries," which confirmed the rejection of the hypothesis that there is a unit root at some level of confidence).

The pairwise causality tests were conducted with the application of the R library MSBVAR, which stands for the Markov-Switching, Bayesian, Vector Autoregression Models (Brandt and Davis, 2014). The application of this library includes the bivariate Granger causality testing for multiple time series. Estimates are found for all possible bivariate G-causality tests for m variables. The test is implemented by regressing Y on p past values of Y and p past values of X. A statistical F-test is then used to determine whether the coefficients of the past values of X are jointly zero. The F-tests are generally based on a decomposition of the variability in data in terms of sums of squares reflecting different sources of variability. In order for the statistic to follow the F-distribution under the null hypothesis, the sums of squares should be statistically independent, and each should follow a scaled chi-squared distribution. The latter condition is guaranteed if the data values are independent and normally distributed with a common variance. This testing produces a matrix with m*(m-1) rows and m columns, which are all of the possible bivariate Granger causal relations. The results include F-statistics and p-values for each pair of variables. The G-causality tests indicate that if X G-cause Y statistically, then it contains the information to help predict future values of Y, and if Y affects X, which is the feedback effect, it means that X and Y are both endogenous, and VAR type model can be used to characterize the interconnection between X and Y.

4. Results and Discussion

The results of calculations of the F-statistic are summarized in Table 3. For the number of variables, m=4 (inlet and outlet gas and liquid pressures), the number of interconnections calculated from m*(m-1) is 12. Table 3 shows that the null hypothesis of the G-causality test of no interconnections of the variables (at the p-value <0.05) is rejected for 10 interconnections, and is accepted for 2 interconnections, indicating no interconnection.

Figure 10 illustrates a multiple bar chart diagram of the F-statistic for the interconnections between the gas and water inlet and outlet pressures measured during the experiment. The chart shows two components for each link, indicating a forward, or

positive, link, and those indicating a backward, or negative, link. The two connections, for which the null hypothesis of no connection is accepted on the *p*-level >0.1, are marked with the asterisk sign.

The data presented in Table 3 and Figure 11 were used to draw a causality loop diagram (CLD) to aid in visualization of how different system's variables are interrelated. The CLD consists of 4 nodes, representing inlet and outlet gas and water ports of the fracture, and the arrows representing the forward and backward links between the nodes. The arrow line widths on the diagram in Figure 11 are proportional to the *F*-statistic values. The dashed lines indicate the links, for which the null hypothesis of no connection is accepted on the *p*-level > 0.1. The CLD represents a closed network of interconnections between variables, indicating system's mutual cause and effect relationships. The CLD is internally initiated by the system properties within the limits of boundary conditions, and the entire temporal and spatial flow processes are connected by causality. For example, starting at the inlet gas pressure, the system's cause-effect propagation can expressed by:

$$g.in \rightarrow l.in \rightarrow l.out \rightarrow g.out \rightarrow g.in \quad (2a)$$

$$g.in \rightarrow l.out \rightarrow g.out \rightarrow g.in \quad (2b)$$

The equations (2) can generally be written for different starting points of the CLD. Table 4 presents the data and Figure 11b show the CLD of the capillary pressure measurements. One can see that the output capillary pressure significantly affects the inlet capillary pressure, which is essentially a confirmation of the initial hypothesis of the influence of the outlet capillary pressure on the inlet capillary pressure. Thus, the results show that, in general, the two-phase fracture flow system exhibits the mutual G-causality properties, because two phases are mutually interacting with each other, which can be considered the default interaction. The connections from Equations 2a and 2b are shown in Figure 12.

Another important point from the results of the causality analysis is related to the definition and measurements of the capillary pressure, which is difficult to measure directly in fracture rock [e.g., Firozabadl and J.Hauge (1990), Reitsma and Kueper, 1994; Faybishenko and Finsterle, 2003]. The capillary pressure is commonly calculated as the difference between the gas (P_{gas}, nonwetting phase) and liquid (P_{liquid}, wetting phase) pressures

$$P_{cap} = P_{gas} - P_{liquid} \quad (3)$$

Equation (3) implies that the pressures are additive variables. However, the dependence of the inlet capillary pressure on the outlet capillary pressure indicates that the capillary pressure calculated from Equation (3) is not a physically based value. The

capillary pressure is in fact a multiplicative variable, intimately dependent on a nonlinear superposition of coupled processes within fractured media. It is very hard if not impossible to categorize the relationship between a "causative agent" and an "effect" of the system components, as coupled processes intimately mix them. (A detailed statistical analysis and a comparison of the calculated and measured capillary pressures are not subject of this paper and will be given in a separate paper.)

As part of the discussion section of the paper, it is important to denote some limitations of the application of the G-causality for the analysis of complex physical situations, as some causes of variation may not be known or observable. The G-causality test is phenomenological, and is based on the analysis of measured variables. This test is basically a measure of the statistical relationship between the variables, and thus can lead to some spurious causalities, if other important relevant variables are not included in the analysis (Hsiao 1982). In this case, the G-causality test may provide a qualitative assessment of the causality and may not necessarily represent true causality. If both X and Y are driven by a conjoint third process with different time lags, one might fail to reject the alternative hypothesis of Granger causality. In this regard, it would be important to manipulate one of the variables to assess the response of the other, which will be conducted in a separate paper based on the analysis of other field and laboratory experiments.

Conclusions and Recommendations

The cause-effect relationships for gas and water pressures affecting flow and transport processes in fractured media, using a conventional statistical regression analysis, are difficult or even impossible to identify, which limit the reliability of numerical modeling and prediction techniques. One of the modern approaches to the evaluation of the cause-effect relationships is the application of the Granger causality principle. The Granger causality statistical approach is based on using predictability as opposed to correlation for detecting interactions between time series variables. In this paper, the proposed approach is tested using the time-series data obtained from the fracture flow experiment conducted by Persoff and Pruess (1995), and initially analyzed in the author's paper (Faybishenko, 2002). In his 2002 paper, based on the visual examination of time series data, the author hypothesized that the observed quasi-periodic pressure oscillations at both inlet and outlet ends of the fracture result from a superposition of both forward and return waves of pressure propagation through the fracture. In the current paper, based on the application of the G-causality test, the author infers that this hypothesis is correct, and demonstrates the causation loop diagram of the spatial-temporal distribution of gas and liquid pressures at the inlet and outlet of the fracture. The evaluation of the gas-water interactions is important to finding the functional significance of monitoring the flow processes. However, because the Granger causality approach is used to analyze responses in measured variables, the method does not identify whether these variables are sufficient to classify causality of the system, or

whether extra variables are required. A physical explanation of the identified statistical causality should be a scope of further research.

The developed CLD can also serve as the basis for the development of the Bayesian network model, with a requirement that the relationships be causal, and for the use of structural equation models (e.g., Greenland and Brumback, 2014; West et al., 1998). The application of causality theory is an innovative framework to hydrological flow and transport investigations, and may take a prominent place as the basis for the development of conceptual and mathematical models, uncertainty evaluation and sensitivity analysis of hydrological and climatic predictions.

Acknowledgement

This material is partially based upon work supported as part of the Sustainable Systems Scientific Focus Area funded by the U.S. Department of Energy, Office of Science, Office of Biological and Environmental Research under Award Number DE-AC02-05CH11231, and the project "Deduce: Distributed Dynamic Data Analytics Infrastructure for Collaborative Environments" of the ASCR DOE program. Constructive comments of two reviewers are very much appreciated. I would like to express my sincere appreciation to Prof. Garrison Sposito for many interesting and encouraging scientific discussions on the topics of nonlinear dynamics and deterministic chaos. In 1990, when late Prof. Paul A. Witherspoon offered me a job at UC Berkeley, he named Gary Sposito as one of the best scientists at UC Berkeley and LBNL.

References

Abarbanel HDI. *Analysis of observed chaotic data*. New York: Springer; 1996.

Bear J, Tsang CF, de Marsily G, editors. Flow and contaminant transport in fractured rock. San Diego, CA: Academic Press; 1993.

Benincà, E., Huisman, J., Heerkloss, R., Jöhnk, K. D., Branco, P., Van Nes, E. H., Scheffer, M., (2008). Chaos in a long-term experiment with a plankton community. *Nature*, 451(7180), 822–825.

Bohm, D. (1957). *Causality and Chance in Modern Physics*, University of Pennsylvania Press, Philadelphia (1957)

Brandt P., Davis W.R. (2014), *Markov-Switching, Bayesian, Vector Autoregression Models (MSBVAR)*, R package, ver. 0.9-1, CRAN repository.

Casini, M. et al., *Proc. Natl. Acad. Sci*. U.S.A. 106, 197 (2009).

Committee on Major U.S. Oceanographic Research Programs, National Research Council, Global Ocean Science: Toward an Integrated Approach (National Academies Press, Washington, DC, 1999).

Cushing, J. M., Costantino, R. F., Dennis, B., Desharnais, R. A., & Henson, S. M. (2003). *Chaos in ecology: Experimental nonlinear dynamics*. San Diego, CA: Academic Press.

Faybishenko, B., Chaotic dynamics in flow through unsaturated fractured media, *Advances in Water Resources* 25 (7), 2002, 793-816 . DOI: 10.1016/S0309-1708(02)00028-3

Faybishenko, B., J. Gale, and S.Benson (editors), *Fluid Dynamics in Complex Fractured-Porous Systems*, 2015, AGU/Wiley. ISBN: 978-1-118-87720-3

Faybishenko, B., P.A.Witherspoon, and J.Gale (editors), *Dynamics of Fluids and Transport in Fractured Rock*, Geophysical Monograph Series, Vol. 162, 2005. [ISBN 0-87590-427-0]

Faybishenko B, Witherspoon PA, Benson SM. (editors). *Dynamics Of Fluids In Fractured Rock*, Geophysical Monograph No 122., Washington DC, 2000.

Gilvear, D.J., M.T. Greenwood, M.C. Thoms, P.J. Wood (editors), *River Science: Research and Management for the 21st Century*, Wiley, 2016.

Gray WG, Hassanizadeh SM. Paradoxes and realities in unsaturated flow theory. *Water Resour Res* 1991;27(8):1847–54.

Greenland, S., B. Brumback (2002). "An overview of relations among causal modelling methods". *International Journal of Epidemiology* **31** (5): 1030–1037.

Guastello, S.J., M.Koopmans, M., D Pincus (eds.), *Chaos and Complexity in Psychology: The Theory of Nonlinear Dynamical Systems*, 2011. Cambridge University Press, ISBN: 9781107680265

Klemeš, V., Empirical and causal models in hydrology, *Studies in Geophysics*, Washington, D.C., 1982.

Lütkepohl, H (2005). New introduction to multiple time series analysis (3 ed.). Berlin: Springer. pp. 41–51. ISBN 3540262393.

May R. M. 1974 Biological populations with nonoverlapping generations: stable points, stable cycles, and chaos. Science 186, 645–647. (doi:10.1126/*Science*.186.4164.645)

MSBVAR: Bayesian estimators and inferences for VAR models, an R package for VAR, BVAR and B-SVAR models. http://yule.utdallas.edu/ Version 0.7, July 2012.

National Research Council Committee on Fracture Characterization and Fluid Flow, Rock fractures and fluid flow: contemporary understanding and applications. Washington, DC: National Academy Press; 1996.

Nicholl MJ, Glass RJ, Wheatcraft SW. Gravity-driven infiltration instability in initially dry non-horizontal fractures. *Water Resour Res* 1994; 30(9):2533–46.

Nicolis JS (1991) *Chaos and Information Processing: A Heuristic Outline*. World Scientific Pub Co Inc

Pasternack GB. Does the river run wild? Assessing chaos in hydrological systems. *Adv Water Res* 1999;23(3):253–60.

Perfect E. Fractal models for the fragmentation of rocks and soils: a review. *Eng Geol* 1997; 48(3–4):185–98.

Persoff P, Pruess K. Two-phase flow visualization and relative permeability measurement in natural rough-walled rock fractures. *Water Resour Res* 1995; 31(5):1175–86.

Pfaff, B., VAR, SVAR and SVEC Models: Implementation Within R Package vars, *Journal of Statistical Software*, July 2008, Volume 27, Issue 4.

Pfaff, B., Analysis of Integrated and Cointegrated Time Series, The 1st International R/Rmetrics User and Developer Workshop, 8–12 July 2007, Meielisalp, Lake Thune, Switzerland.

Pruess K, Faybishenko B, Bodvarsson GS. Alternative concepts and approaches for modeling flow and transport in thick unsaturated zones of fractured rocks. *J Contam Hydrol* 1999;38:281–322 [special issue].

Rabinovich MI, Trubetskov DI. *Oscillations and waves in linear and nonlinear systems*. The Netherlands: Kluwer Academic Publishers; 1994.

Schuster HG. *Deterministic chaos: an introduction*. Weinheim: Federal Republic of Germany, New York: Physik-Verlag; 1989.

Scientific Basis Of Water-Resource Management, Geophysics Study Committee, Geophysics Research Board, Assembly Of Mathematical And Physical Sciences, National Research Council, National Academy Press, Washington, Dc L982.

Sivakumar B. Chaos theory in hydrology: important issues and interpretations. *J Hydrol* 2000; 227:1–20.

Skarda CA, Freeman WJ (1987) How brains make chaos in order to make sense of the world. *Behavioral & Brain Sci* 10: 161–195.

Spirkin, A. (1990), *Fundamentals of Philosophy*. Translated from the Russian by Sergei Syrovatkin. Moscow: Progress Publishers.

Sposito G. On chaotic flows of water in the vadose zone. *Abstracts of the Fall 1999 AGU Meeting*, December 1999.

Sugihara, G., R. M. May, *Nature* 344, 734 (1990).

Sugihara, G., R.May, H.Ye, C.-H.Hsieh, E.Deyle, M.Fogarty, S.Munch, Detecting Causality in Complex Ecosystems, 2012 VOL 338 *Science*.

Weeks SW, Sposito G. Mixing and stretching efficiency in steady and unsteady groundwater flows. *Water Resour Res* 1998; 34(12): 3315–22.

West, S. G, Finch, J. F., & Curran, P. J. (1995). Structural equation models with non-normal variables: Problems and remedies. In R. H. Hoyle (Ed.), Structural equation modeling: Concepts, issues, and applications (pp. 56−75). Thousand Oaks, CA: Sage.

Winfree, A.T., The prehistory of the Belousov-Zhabotinsky oscillator, *J. Chem. Educ*., 1984, 61 (8), p 661, DOI: 10.1021/ed061p661

Figures

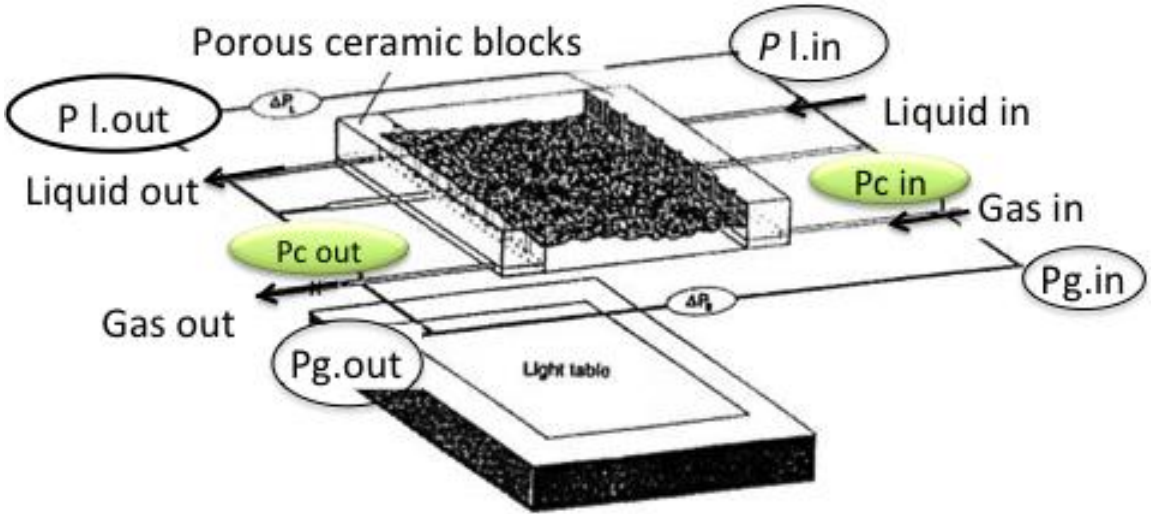

Figure 1. A schematic diagram of the fracture flow experiment used for investigating two-phase flow regime in rock fracture specimen [66]. Ovals represent four absolute and four differential pressure transducers (Persoff and Pruess, 1995).

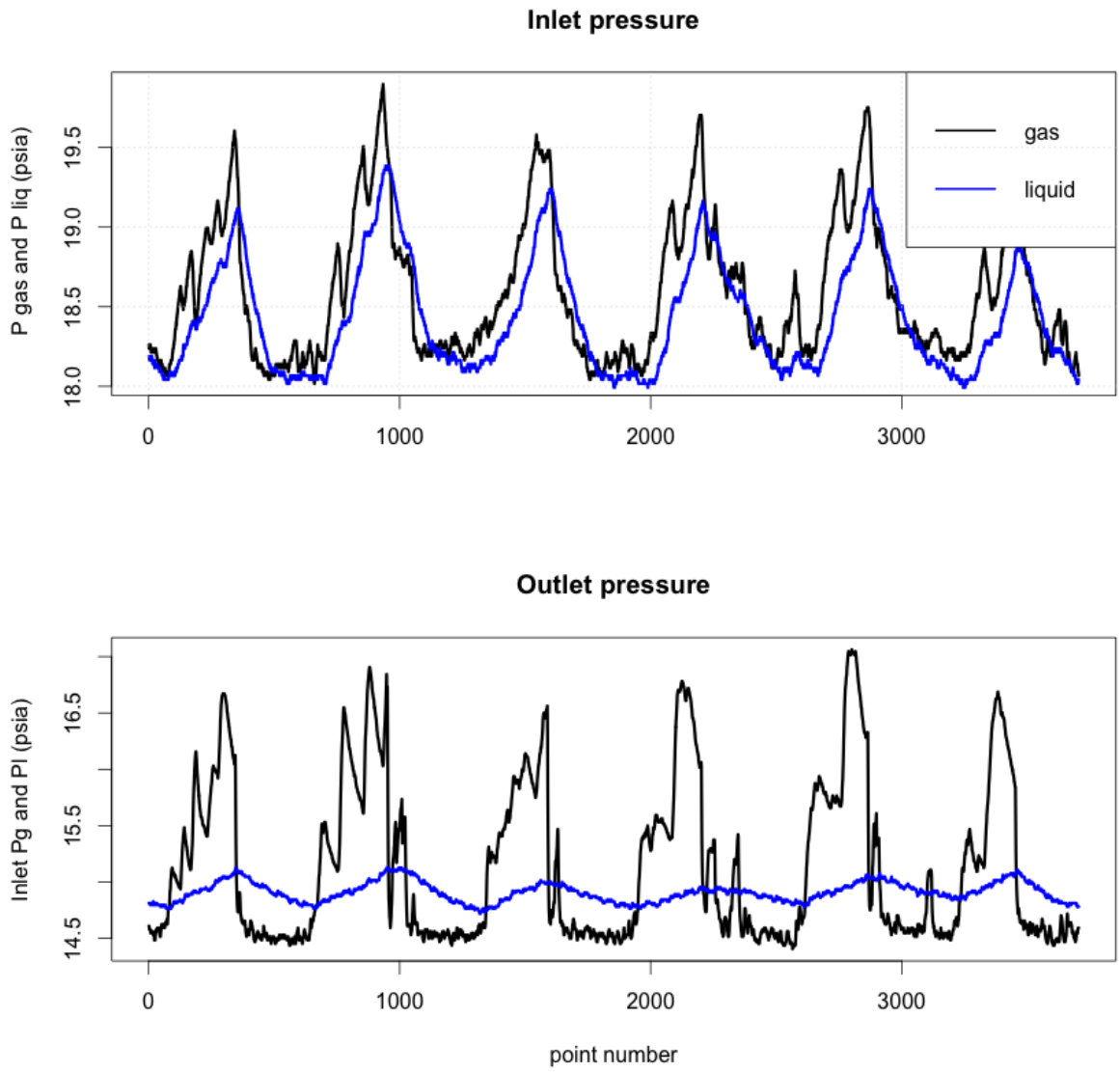

Figure 2. Time series of inlet and outlet gas and liquid pressures measured during the fracture flow experiment shown in Figure 1.

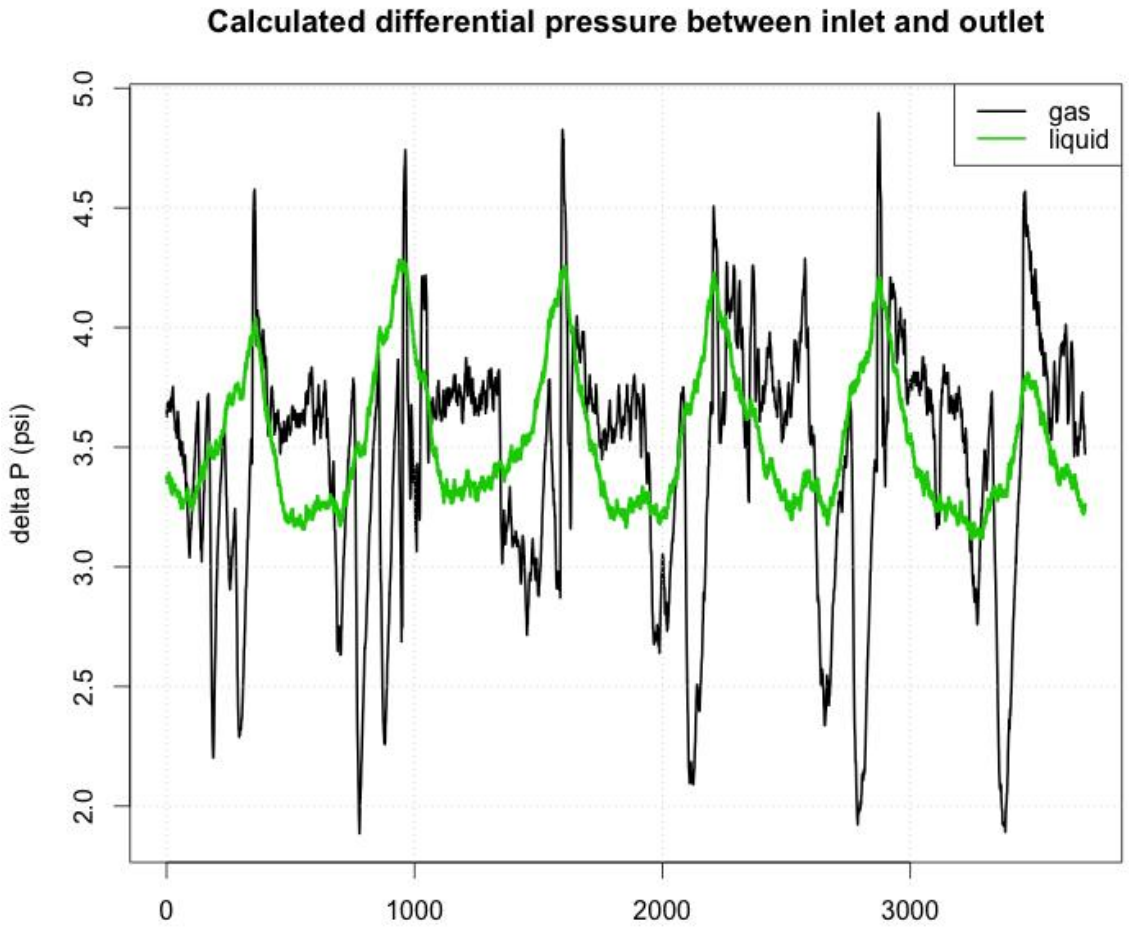

Figure 3. Differential gas and liquid pressures along the length of the fracture (calculated as a difference between inlet and outlet gas pressures, and as a difference between the inlet and outlet liquid pressures).

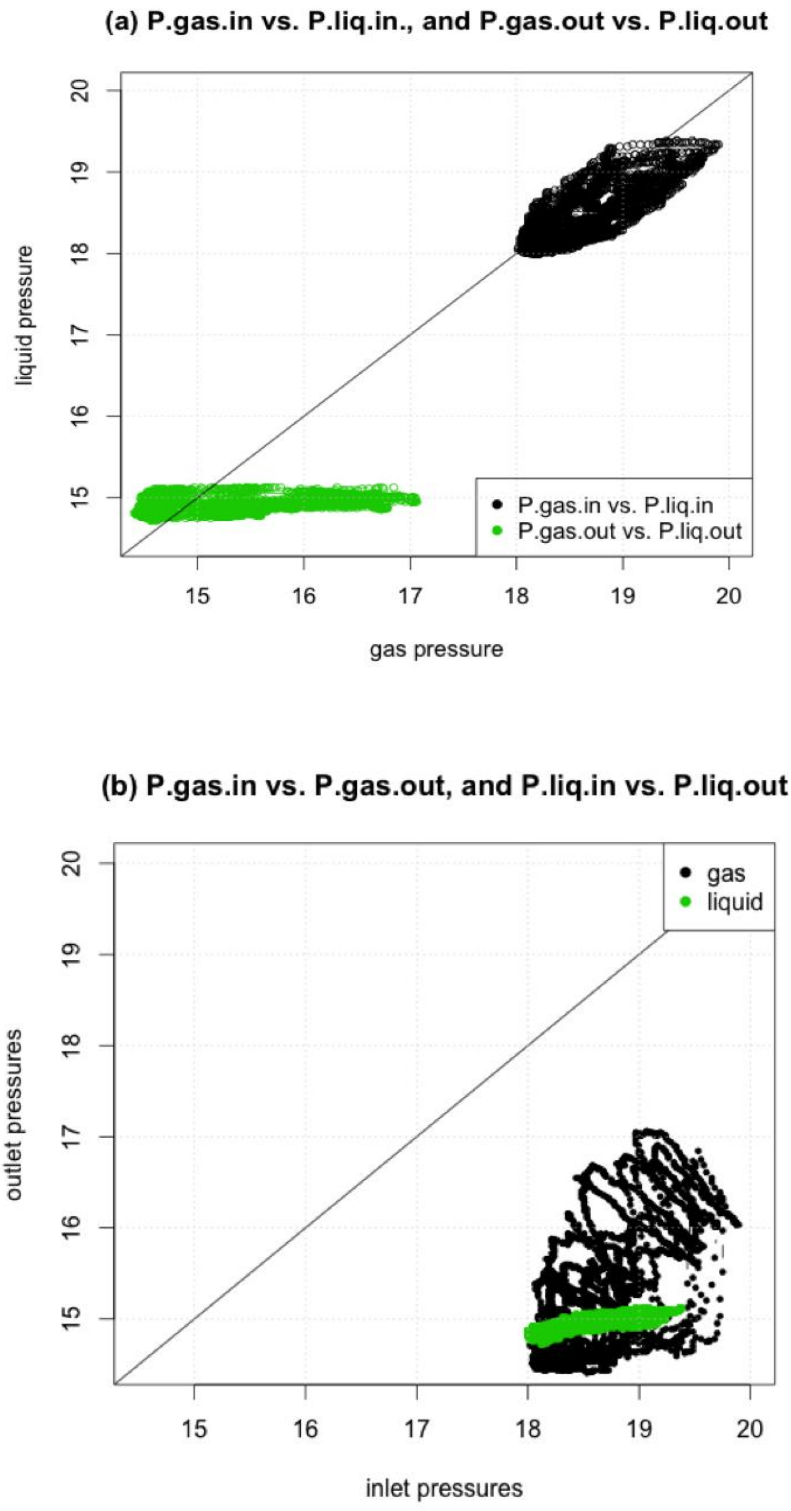

Figure 4. 2D phase-space attractors/scatterplots of measures pressures (using time series data in psi shown in Figure 2): figure (a) – black points: $P_{gas.in}$ vs $P_{liq.in}$, and green points: $P_{gas.out}$ vs $P_{liq.oot}$; and figure (b) – black points: $P_{gas.in}$ vs $P_{gas.out}$ and green points: $P_{liq.in}$ vs $P_{liq.out}$.

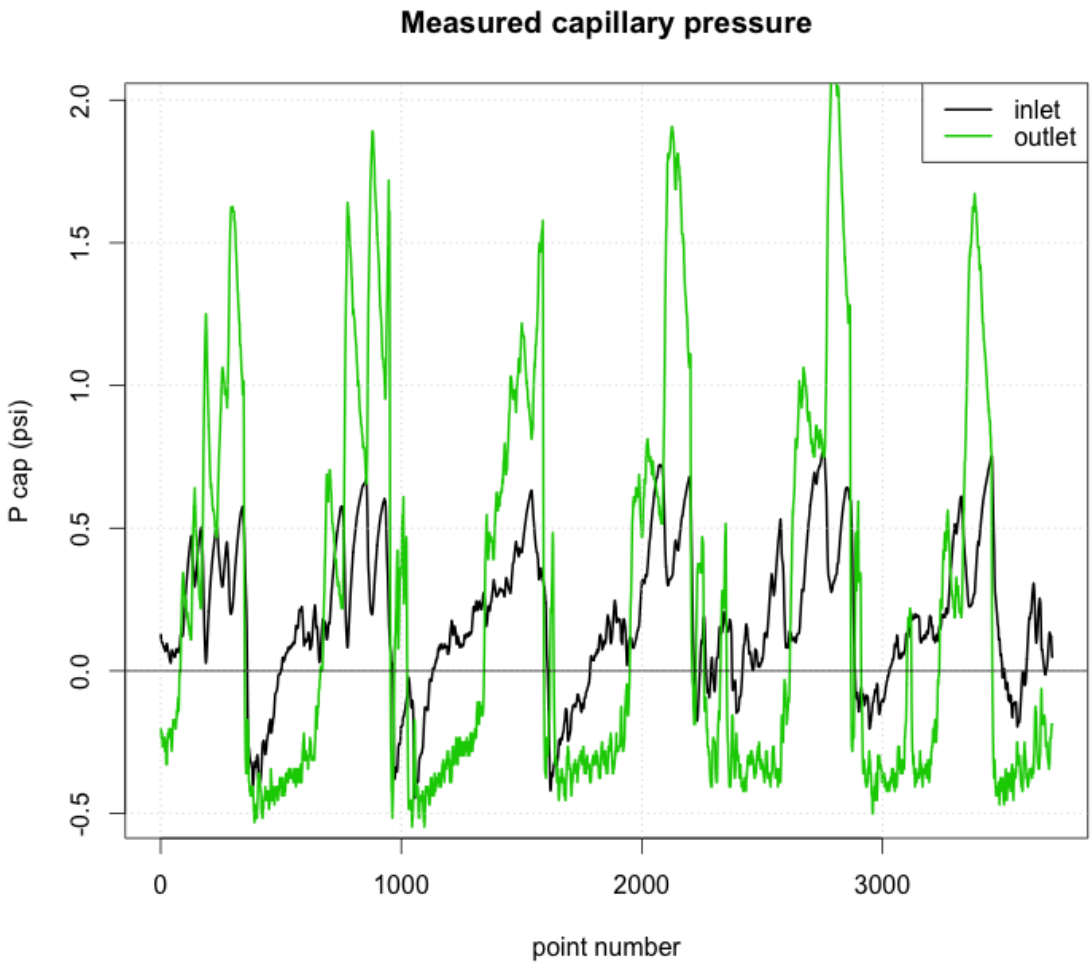

Figure 5. Capillary pressure at the inlet and outlet of the fracture (measured using differential manometers as the difference between pressures at the gas and liquid ports). P_{cap} is calculated using Eq. (3)

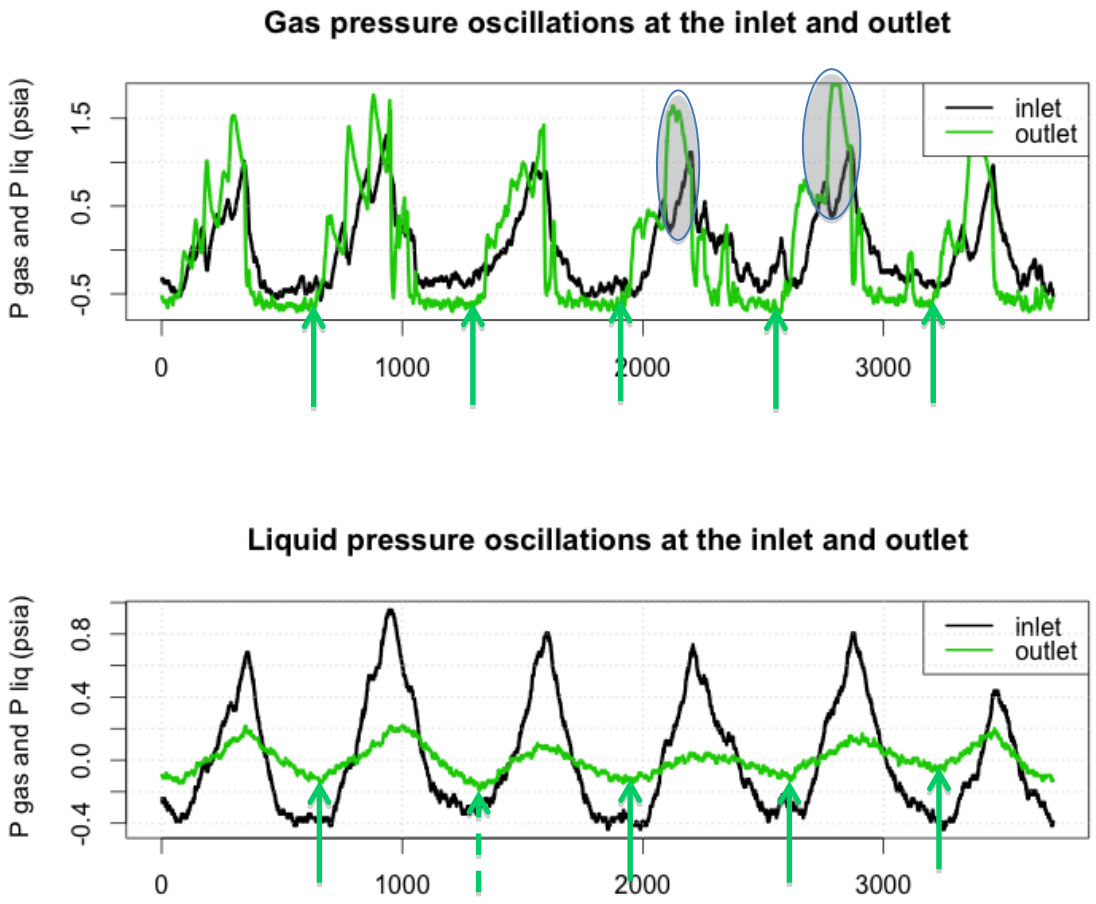

Figure 6. Inlet and outlet gas and liquid pressure oscillations (calculated as the difference between the measured and mean values for each time series), showing by the arrows that the pressure changes began first at the outlet following by the changes at the inlet (a single contrary instance is indicated by a dashed vertical line). Ovals on the upper figure indicate the periods of reverse changes in the gas pressure.

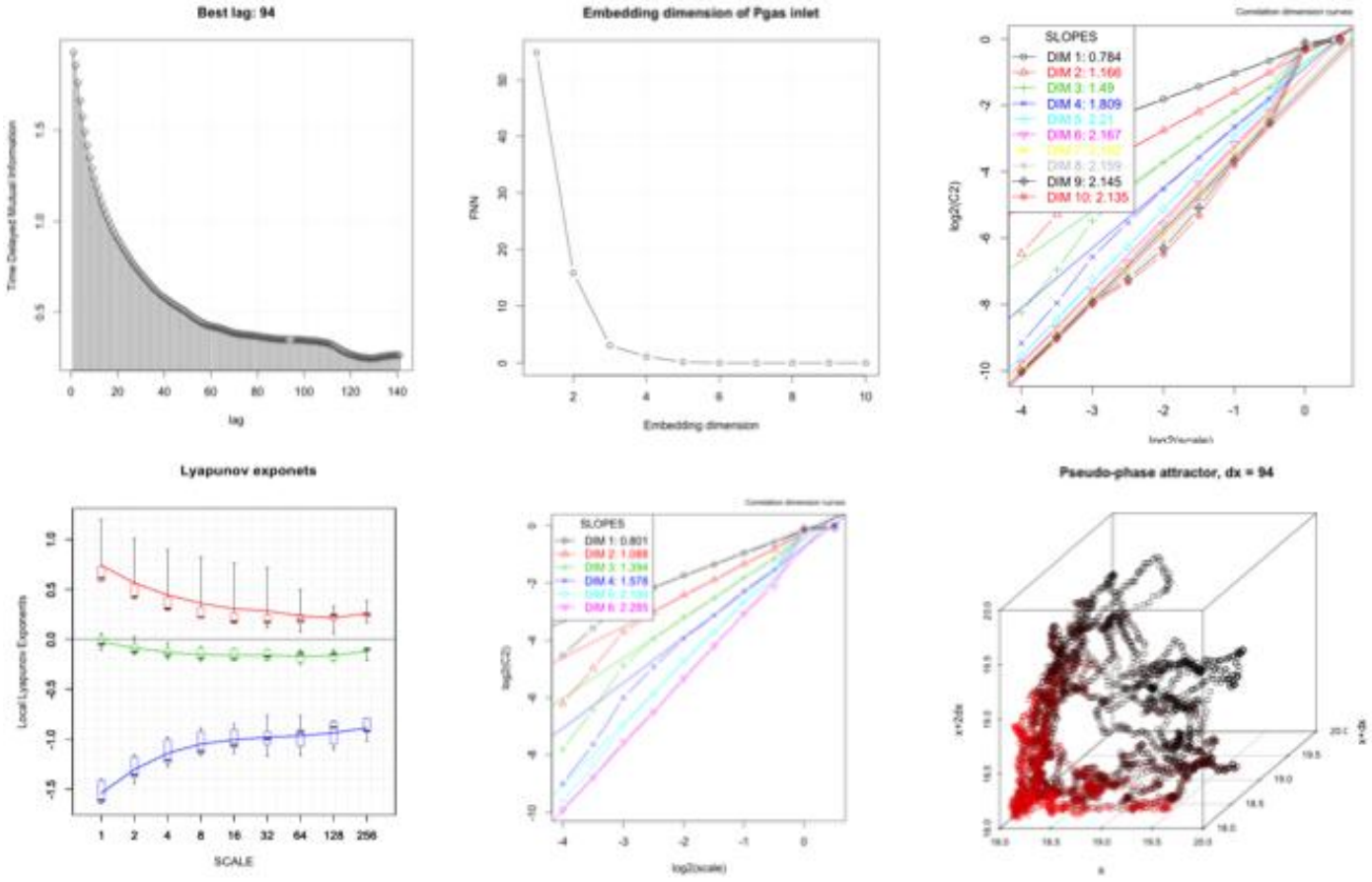

Figure 7. Results of the evaluation of chaotic parameters of inlet gas pressure: upper row from left to right—averaged mutual information to determine the time delay, embedding dimension determined using the False Nearest Neighbor (FNN) method, and correlation dimension (D2), and the lower row—Lyapunov exponents, information dimension, and 3D pseudo-phase space attractor.

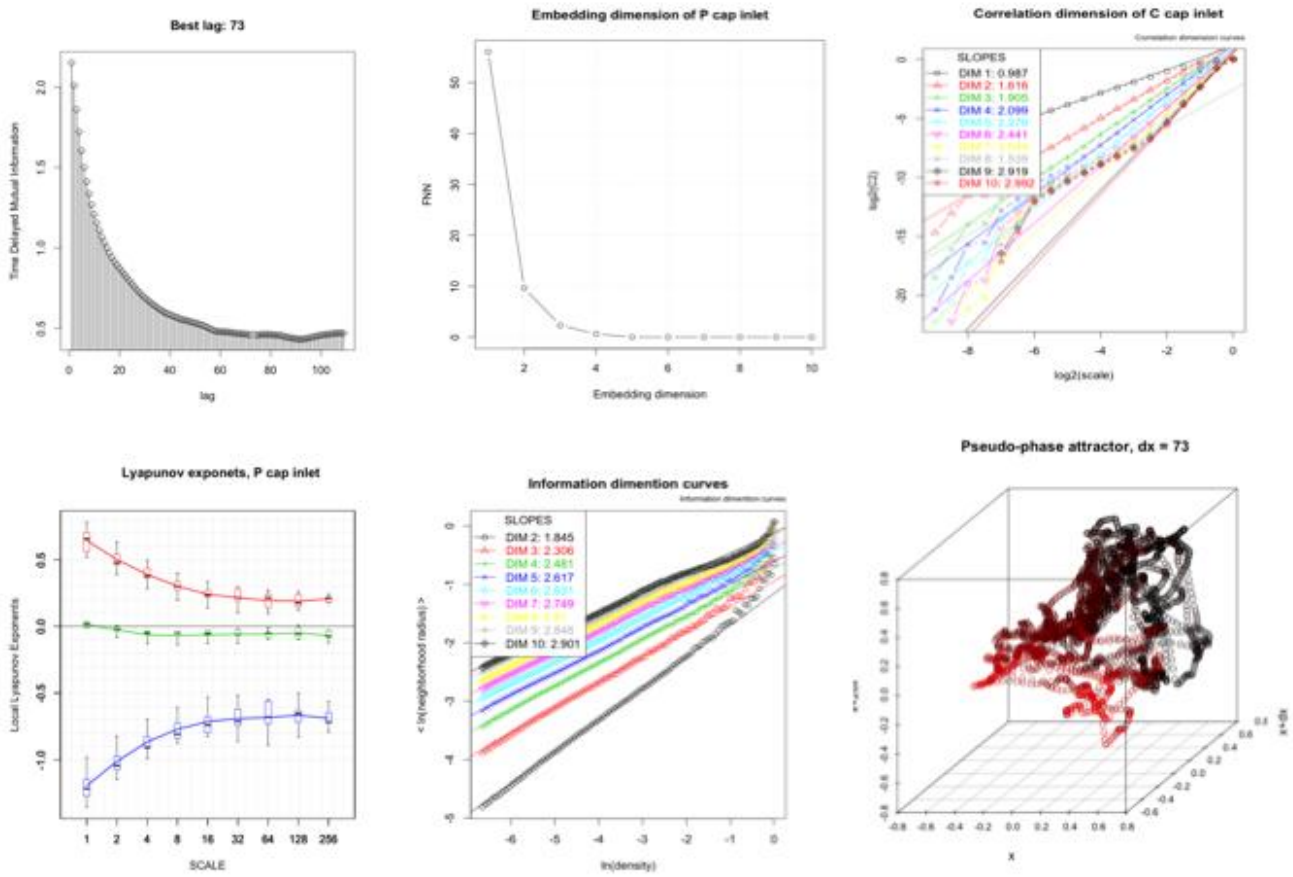

Figure 8. Results of the evaluation of chaotic parameters of out gas pressure: upper row from left to right—averaged mutual information to determine the time delay, embedding dimension determined using the False Nearest Neighbor (FNN) method, and correlation dimension (D2), and the lower row—Lyapunov exponents, information dimension, and 3D pseudo-phase space attractor.

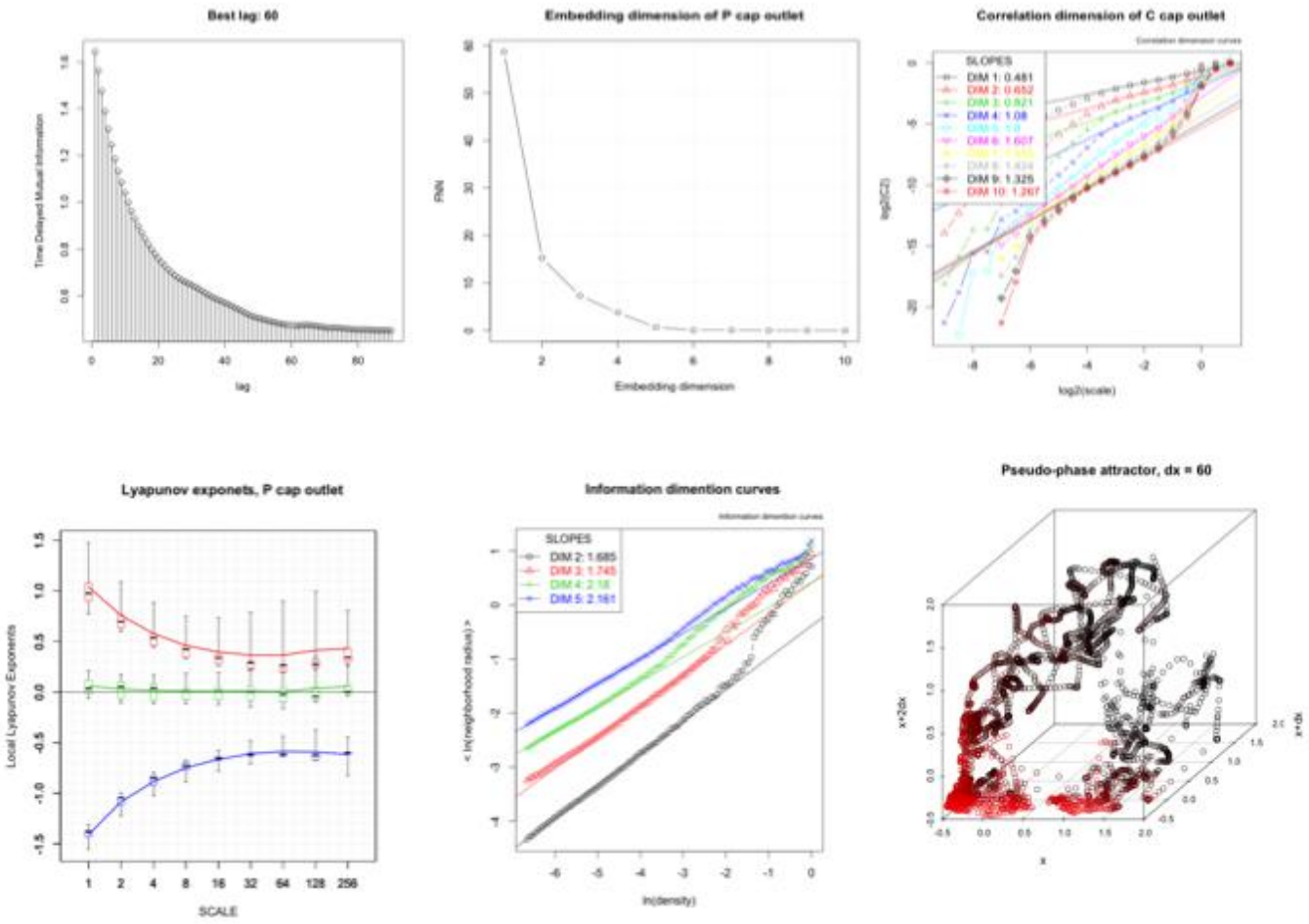

Figure 9. Results of the evaluation of chaotic parameters of inlet capillary pressure: upper row from left to right—averaged mutual information to determine the time delay, embedding dimension determined using the False Nearest Neighbor (FNN) method, and correlation dimension (D2), and the lower row—Lyapunov exponents, information dimension, and 3D pseudo-phase space attractor.

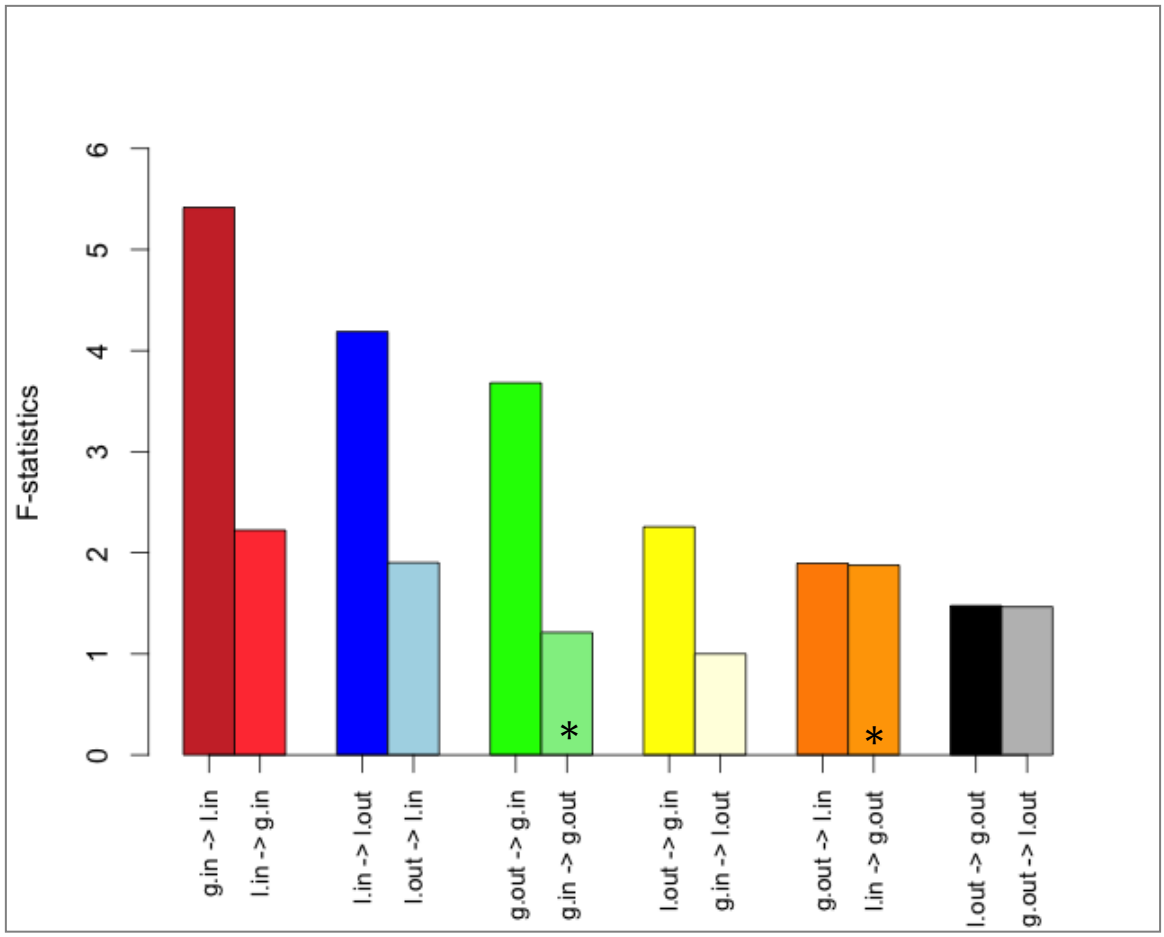

Figure 10. Bar chart of the *F*-statistics calculated from the time series measurements of gas and water inlet and outlet pressures for the fracture flow experiment. The two connections, for which the null hypothesis of no connection is accepted on the *p*-level of >0.1, are indicated with the asterisk sign. On Figures 10-12: g.in – gas pressure at the inlet gas port, l.in – liquid pressure at the inlet liquid port, g.out –gas pressure at the outlet gas port, and l.out – liquid pressure at the outlet liquid port.

(a)

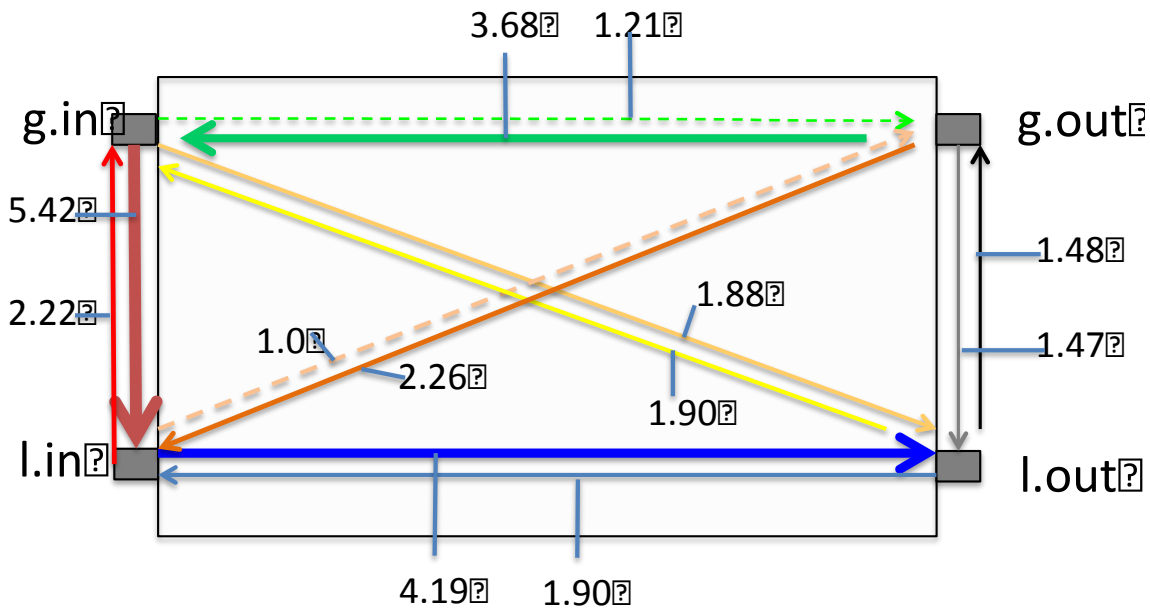

(b)

Figure 11. (a) Causality loop diagram showing *F*-statistics values (numbers on the diagram) of the interconnections of the inlet and outlet gas and liquid pressures. Solid lines indicate that the null hypothesis for independence is rejected (*p*-values <0.05), and dashed lines – the null hypothesis of independence is accepted at the *p*-value level >0.1. (b) The same for the measured capillary pressures.

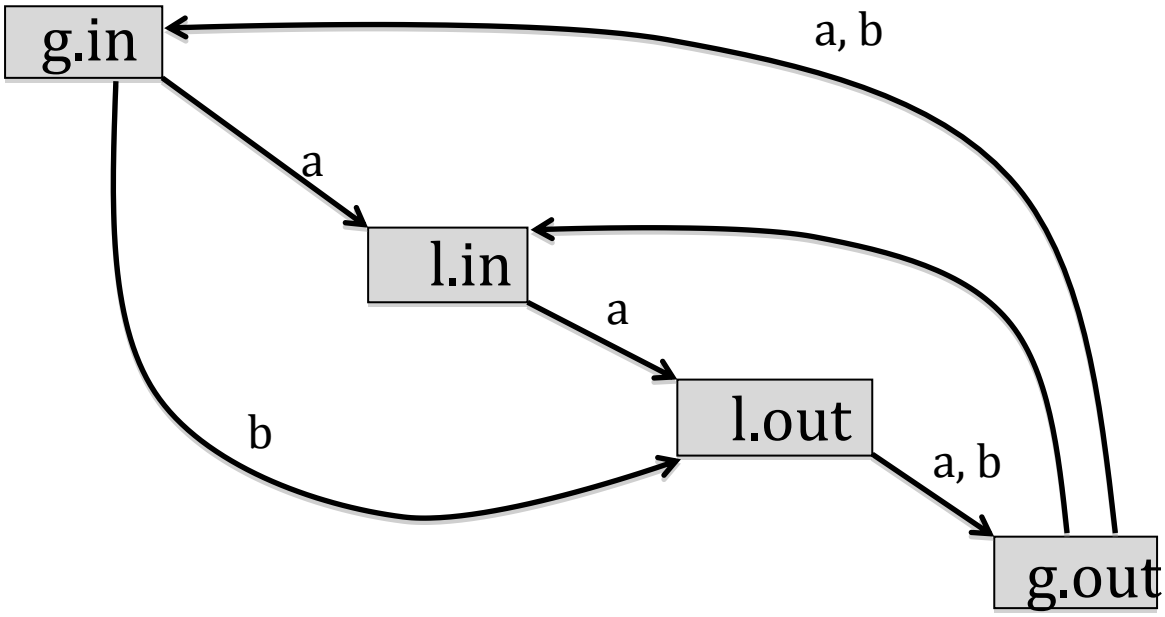

Figure 12. An acyclic graph of the prevailing causalities taken from the CLD on Figure 11. (a) and (b) indicate the connections from Equations 2a and 2b.

Table

Table 1. Diagnostic parameters of chaos

Time series	AMI (time delay)	Embedding dimention (D_{EMD})	Correlation dimension D_{cor}	Max Lyapunov exponent	Sum of Lyapunov exponents	Information dimension D_{inf}
$P_{g.in}$	94 / 89	5	1.85	0.25	-0.77	2.03
$P_{l.in}$	181 / 178	4	1.57	0.21	-1.16	2.51
$P_{cap.in}$	73 /61	4	2.62	0.21	-0.58	2.72
$P_{cap.out}$	66 / 60	4	2.17	0.34	-0.26	2.87

Note: Time delay values are given: in the nominator—measured data, in the dominator–noise removed data.

Table 2. KPSS Unit Root Test shows that the null hypothesis of stationarity should be accepted as the values of the test statistics given in table (a) are less than the 10%, 5% and 1% critical values given in table (b).

(a)

Variable	**Value of test-statistic**
$P_{g.in}$	0.0388
$P_{l.in}$	0.0291
$P_{g.out}$	0.0394
$P_{l.out}$	0.0952
$P_{c.in}$	0.0405
$P_{c.out}$	0.05

(b)

Significant level	Critical value
1%	0.216
2.5%	0.176
5%	0.146
10%	0.119

Table 3. Results of the Multivariable G-causality test

G-causality	F-statistics	*p*-value	Accept/Reject
$P_{l.in} \rightarrow P_{g.in}$	2.224	9.35E-09	Reject
$P_{g.out} \rightarrow P_{g.in}$	3.681	0	Reject
$P_{l.out} \rightarrow P_{g.in}$	1.896	5.69E-06	Reject
$P_{g.in} \rightarrow P_{l.in}$	5.417	0	Reject
$P_{g.out} \rightarrow P_{l.in}$	2.257	4.71E-09	Reject
$P_{l.out} \rightarrow P_{l.in}$	1.902	5.09E-06	Reject
$P_{g.in} \rightarrow P_{g.out}$	1.212	0.103	Accept
$P_{l.in} \rightarrow P_{g.out}$	1.001	0.476	Accept
$P_{l.out} \rightarrow P_{g.out}$	1.476	4.91E-03	Reject
$P_{g.in} \rightarrow P_{l.out}$	1.877	8.01E-06	Reject
$P_{l.in} \rightarrow P_{l.out}$	4.188	0	Reject
$P_{g.out} \rightarrow P_{l.out}$	1.466	5.68E-03	Reject

Table 4. Causality of the bidirectional G-causality test for inlet and outlet capillary pressures (measured and noise removed)

G-causality	Measured data		Noise removed data	
	F-statistics	*p*-value	F-statistics	*p*-value
$P_{cap.out} \rightarrow P_{cap.in}$	3.966	0	2.595	1. 1e-10
$P_{cap.in} \rightarrow P_{cap.out}$	1.672	0.0006	1.288	0.062